Online Identification Method of Distribution Line-to-ground Parameters and Grounding Transition Conductance During Arc Suppression

Zeyin Zheng, Jianfeng Xu, and Moufa Guo

***Abstract*—Since the effectiveness of the flexible current arc suppression method heavily relies on the accurate measurement of the distribution line-to-ground parameters, the suppression of single line-to-ground (SLG) fault current may deteriorate due to factors such as line switching and other disturbances during SLG fault arc suppression. Additionally, during SLG fault arc suppression, promptly identifying the fault type and rapidly deactivating the flexible arc suppression device (FASD) can reduce the overvoltage risk in non-faulted phase devices. To address these issues, this paper presents a parameter identification method based on recursive least squares (RLS) while a variable forgetting factor strategy is introduces to enhance the RLS algorithm's disturbance rejection capability. Simulations verify that the variable forgetting factor recursive least squares (VFF-RLS) algorithm can accurately identify distribution line-to-ground parameters in real time and effectively suppress SLG fault current. The online identification of grounding transition conductance is simultaneously used to determine the fault type and quickly detect when the SLG fault has been cleared.**

***Index Terms*—Distribution networks, single line-to-ground fault arc suppression, distribution line-to-ground parameters grounding transition conductance, recursive least square method, online identification.**

I. Introduction

Distribution networks have complex line structures, which expose them to random faults. Among the different types of faults, SLG faults are the most common, accounting for approximately 80% of the total [1], [2]. With the proportion of cable lines in the distribution network increasing and the installation of increased numbers of nonlinear-power electronic devices [3], the fault current during SLG faults keeps increasing. The traditional neutral point grounding method using arc suppression coils struggles to meet arc suppression requirements [4]. If the SLG fault current is not promptly suppressed, a SLG fault could potentially escalate and even jeopardize personal safety, thus making reliable arc suppression critically important.

Existing arc suppression methods generally achieve their goal by regulating arc-suppression devices to compensate for fault point currents [5]. These can be categorized as passive, active, and hybrid arc suppression devices [6]–[8]. Among them, passive arc suppression devices are represented by arc suppression coils, while hybrid and active arc suppression devices focus on compensating current, whereas all require accurate measurement of distribution line-to-ground parameters. This is crucial for enhancing the reliability of arc suppression, as the effectiveness of these devices is closely tied to the precision of distribution line-to-ground parameters measurement.

Traditional methods of measuring distribution line-to-ground parameters can be classified as offline measurements, which obtain the parameters offline by injecting specific frequency currents combined with relevant algorithms under normal system operation conditions [9]. The line-to-ground parameter information used in the existing current arc suppression method must be identified online by injecting a specific frequency current through an additional device, thereby increasing the cost and impacting the distribution network. A hybrid flexible arc suppression device (HFASD) is introduced that incorporates a second-order generalized integrator phase-locked loop (SOGI-PLL) algorithm and utilizes a twice-injection current method [10]. This approach is designed to precisely measure insulation parameters under the typical operating conditions of distribution networks. However, using the offline-measured distribution line-to-ground parameter values for arc suppression may not adapt well to changes that occur in the distribution line-to-ground parameters during SLG faults [11]. This limitation becomes evident when factors such as line switching and

Received: July 20, 2024
Accepted: November 16, 2024
Published Online: July 1, 2025

Zeyin Zheng (corresponding author) is with the College of Electrical Engineering and Automation, Fuzhou University, Fuzhou 350108, China; and Fuzhou University ZHICHENG College, Fuzhou 350002, China (e-mail: zhengzeyin@fzu.edu.cn).

Jianfeng Xu is with the College of Electrical Engineering and Automation, Fuzhou University, Fuzhou 350108, China (e-mail: 1309944960@qq.com).

Moufa Guo is with the College of Electrical Engineering and Automation, Fuzhou University, Fuzhou 350108, China; and Engineering Research Center of Smart Distribution Grid Equipment, Fujian Province University, Fuzhou 350108, China (e-mail: gmf@fzu.edu.cn).

DOI: 10.23919/PCMP.2024.000174

abnormal adjustments of arc suppression coils occuring during arc suppression [12], [13]. Online parameter measurement overcomes the drawbacks of offline methods by dynamically sensing changes in system parameters, such as line switching and abnormal adjustments of arc suppression coils and updating measurement results in real time. This capability effectively prevents an increase in residual fault currents.

However, research regarding online identification of line-to-ground parameters in distribution networks, is limited. Therefore, insights can be drawn from more mature research, e.g., on inverters and permanent magnet synchronous motors, to guide the online identification of line-to-ground parameters in distribution networks. Meanwhile, existing fault type discrimination methods struggle to identify grounding transition conductance in real time, typically relying on reducing the injected current and observing the proportional relationship between zero-sequence voltage and zero-sequence current to determine whether a fault is permanent or transient. This method of discriminating is indirect and has limited accuracy. In addition, for permanent fault, reducing the injected current may increase the SLG fault current, thus posing a safety risk. Real-time estimation of the grounding transition conductance value through online identification methods, would allow the fault type to be quickly determined by observing the correlation between the online identified grounding transition conductance value and the set threshold.

Existing online parameter identification methods include the Kalman filter method, model adaptive method, and recursive least squares method, etc. [14]–[16]. The Kalman filter method is based on the state equation of a linear system and involves collecting input and output data to achieve optimal state estimation. The model adaptive method utilizes the actual system as a benchmark and constructs a reference using the system's mathematical model for the unknown parameters. The goal is to adjust these unknown parameters, often using the first and second Lyapunov methods for adaptive adjustment to ensure the output aligns with the actual model. The least squares method aims to minimize the sum of squared errors to derive optimal parameters [17]. While it can easily estimate parameters, in practice, as the sample size increases, the dimensions of the computation matrix may exceed the controller's processing capacity. Therefore, the recursive least squares (RLS) method is developed in [18], requiring only one new data point for each update. This method is widely used for online parameter identification. Additionally, the RLS algorithm allows the forgetting factor to be adjusted according to requirements, while a adequate forgetting factor setting allows the algorithm to exhibit both high identification accuracy and excellent disturbance rejection performance [19], [20]. Hence, this study employs the RLS method for online parameter identification while its performance is enhanced through a variable forgetting factor strategy.

The main contributions of this paper are:

1) Based on the zero-sequence equivalent circuit during normal operation of the distribution network, the study derives online identification equations for the line-to-ground parameters using the RLS method. Additionally, building upon this foundation and applying the superposition theorem to the zero-sequence equivalent circuit during an SLG fault in the distribution network, the study derives online identification equations for the line-to-ground parameters and grounding transition conductance using the RLS algorithm.

2) In consideration of the impact of variations in line operating conditions on online identification, the study introduces a variable forgetting factor (VFF) strategy to enhance the anti-interference ability of the RLS algorithm. Simulation results indicate that the VFF-RLS algorithm accurately identifies line-to-ground parameters and grounding transition conductance, demonstrating faster parameter identification convergence and superior arc suppression compared to the RLS algorithm.

The rest of the paper is organized as follows. Section II briefly introduces the principle of SLG fault arc suppression based on the current arc suppression method. Section III presents an online identification method for distribution line-to-ground parameters and grounding transition conductance based on RLS, and proposes a variable forgetting factor strategy to enhance the RLS algorithm's adaptability to dynamic scenarios. In Section IV, simulations are conducted to verify the effectiveness of online identification of the distribution line-to-ground capacitance and grounding transition conductance based on the VFF-RLS algorithm, which confirms that the VFF-RLS algorithm exhibits faster parameter identification convergence and more effective arc suppression than the RLS algorithm. Finally, Section V summarizes the findings and conclusions.

II. Principle of Flexible Neutral Point Arc Suppression Based on Current Arc Suppression Method

A. Distribution Network with an FASD

Figure 1 shows the diagrams of the arc suppression structure for a SLG fault in a distribution network with an FASD. As shown, G represents the ideal power supply at 110 kV, while the distribution network voltage is transformed from 110 kV to 10.5 kV via the transformer T_{yd}. The FASD comprises a cascade H-bridge (CHB) converter and filter inductor L_H, and is connected between the neutral point N formed by the zigzag transformer T_{zt} and ground. The neutral point voltage of the distribution network is denoted as u_N. Assuming that an SLG fault occurs in phase A, the voltage of the

faulty phase is denoted as $u_f = u_A$. The line-to-ground currents are $i_{A\Sigma}$, $i_{B\Sigma}$ and $i_{C\Sigma}$; u_A, u_B, and u_C are the phase-to-ground voltages; r_{0A}, r_{0B} and r_{0C} represent the line-to-ground resistances; c_{0A}, c_{0B}, and c_{0C} denote the line-to-ground capacitances; R_f and g_f represent the grounding transition resistance and grounding transition conductance, respectively; and i_f is the SLG fault current. The injected current and output voltage of FASD are denoted as i_H and u_H, respectively. The SOGI-PLL module extracts the amplitude and phase of the target [1]. The output of the VFF-RLS module used in (23), identifies the line-to-ground parameters g_0, C_0, and grounding transition conductance g_f. The proportional integral differential (PID) module and improved distributed commutations modulation (IDCM) module are respectively responsible for controlling and modulating the injected current i_H of the FASD [21]. This enables the injected current i_H of the FASD to track the reference current i_{ref} calculated by (4).

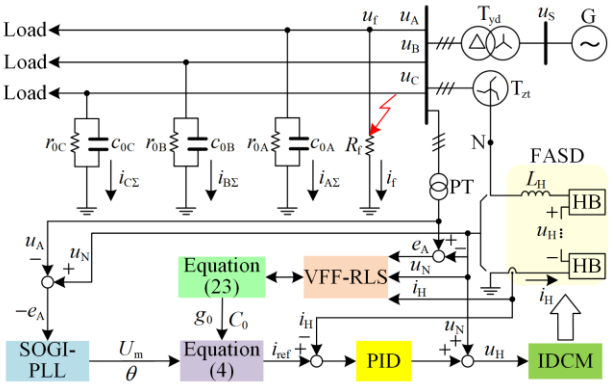

Fig. 1. SLG fault arc suppression structure diagram of distribution network with FASD.

B. Principle of Current Arc Suppression Method

According to Kirchhoff's current law (KCL), the injected compensating current i_H in Fig. 1 can be represented by:

$$i_H = i_{A\Sigma} + i_{B\Sigma} + i_{C\Sigma} + i_f = \frac{u_A}{r_{0A}} + c_{0A}\frac{du_A}{dt} + \frac{u_B}{r_{0B}} + c_{0B}\frac{du_B}{dt} + \frac{u_C}{r_{0C}} + c_{0C}\frac{du_C}{dt} + \frac{u_A}{R_f} \tag{1}$$

Assuming that the line-to-ground parameters are symmetrical, the total line-to-ground resistance can be defined as $1/r_0 = 1/r_{0A} + 1/r_{0B} + 1/r_{0C}$, and the total line-to-ground capacitance can be defined as $C_0 = c_{0A} + c_{0B} + c_{0C}$. The faulty phase supply voltage is denoted as e_A. Therefore, the zero-sequence equivalent circuit diagram of Fig. 1 is depicted in Fig. 2.

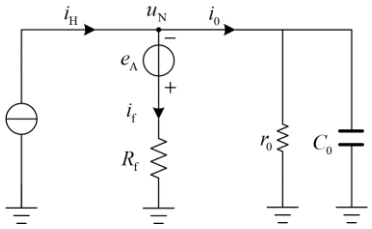

Fig. 2. The zero-sequence equivalent circuit for SLG fault in the distribution network.

According to KCL, the injected compensating current i_H in Fig. 2 can be represented by:

$$i_H = i_0 + i_f = \frac{u_N}{r_0} + C_0\frac{du_N}{dt} + \frac{u_N + e_A}{R_f} \tag{2}$$

By replacing $u_N + e_X = u_X$, $X = A, B, C$ into (2), the injected compensating current i_H can be represented by:

$$\begin{aligned} i_H &= \frac{u_N}{r_0} + C_0\frac{du_N}{dt} + \frac{u_A}{R_f} = \\ &\frac{1}{r_0}(u_A - e_A) + C_0\frac{d(u_A - e_A)}{dt} + \frac{u_A}{R_f} = \\ &\frac{u_A}{r_0} + C_0\frac{du_A}{dt} - \left(\frac{e_A}{r_0} + C_0\frac{de_A}{dt}\right) + \frac{u_A}{R_f} \end{aligned} \tag{3}$$

When the injected compensating current i_H satisfies:

$$i_H = i_{ref} = -\left(\frac{e_A}{r_0} + C_0\frac{de_A}{dt}\right) \tag{4}$$

The faulty phase voltage u_A can be limited to 0, indicating that the SLG fault residual current is suppressed to 0. Hence, the arc associated with the SLG fault can be extinguished.

III. Principle of the Online Identification Method

Based on the analysis presented in Section II, accurate identification of the line-to-ground parameters is crucial in determining the magnitude of the injected current, which significantly influences the effectiveness of arc suppression. In this section, the equivalent circuit diagram and parameter identification formulas are analyzed and deduced for both normal and SLG fault operating conditions. Moreover, it introduces an improvement to the traditional RLS algorithm by using a variable forgetting factor strategy to enhance the online identification performance.

A. RLS Algorithm During Normal Operating Conditions

The zero-sequence equivalent circuit diagram during normal operation of the distribution network is shown in Fig. 3.

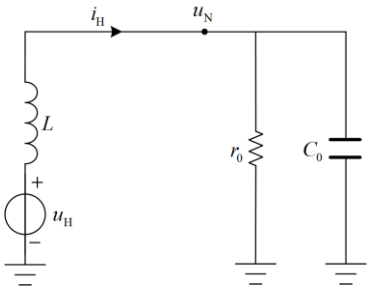

Fig. 3. The zero-sequence equivalent circuit diagram during normal operation.

According to KCL, the injected compensating current i_H in Fig. 3 can be represented by:

$$i_H = \frac{u_N}{r_0} + C_0 \frac{du_N}{dt} \tag{5}$$

The total line-to-ground conductance can be defined as $g_0 = 1/r_0$. Applying the Laplace transformation on (5) yields:

$$i_H(s) = \frac{u_N(s)}{r_0} + sC_0 u_N(s) = (g_0 + sC_0)u_N(s) \tag{6}$$

where system input $u(s) = i_H(s)$; and system output $y(s) = u_N(s)$. Therefore, the transfer function of the system is:

$$H(s) = \frac{u_N(s)}{i_H(s)} = \frac{1}{g_0 + sC_0} \tag{7}$$

The pulse transfer function of an open-loop system with a zero-order holder is given by:

$$H(z) = \frac{z^{-1}}{g_0} \frac{1 - e^{-g_0 T_c / C_0}}{1 - z^{-1} e^{-g_0 T_c / C_0}} = \frac{u_N(z)}{i_H(z)} \tag{8}$$

where T_c is the sampling period, as deduced from (8):

$$u_N(k) = \frac{1 - e^{-g_0 T_c / C_0}}{g_0} i_H(k-1) + e^{-g_0 T_c / C_0} u_N(k-1) \tag{9}$$

Simplifying the coefficients of the injected current i_H and the neutral point voltage u_N in (9), let $a = (1 - e^{-g_0 T_c / C_0})/g_0 = (1+b)/g_0$, $b = -e^{-g_0 T_c / C_0}$, then equation (9) can be rearranged as:

$$u_N(k) = a i_H(k-1) - b u_N(k-1) \tag{10}$$

Due to T_c being the sampling period with a very small value approaching 0, utilizing the equivalent infinitesimal formula, it can be inferred that:

$$\begin{cases} \lim\limits_{T_c \to 0} a = \lim\limits_{T_c \to 0} \dfrac{1 - e^{-g_0 T_c / C_0}}{g_0} = \dfrac{1}{g_0} \dfrac{g_0 T_c}{C_0} = \dfrac{T_c}{C_0} \\ \lim\limits_{T_c \to 0} b = \lim\limits_{T_c \to 0} (-e^{-g_0 T_c / C_0}) = -1 \end{cases} \tag{11}$$

Therefore, based on the parameter identification results a and b, the identification formulas for line-to-ground conductance and line-to-ground capacitance of the distribution network can be stated as follows:

$$g_0 = (1+b)/a, \; C_0 \approx T_c / a \tag{12}$$

B. RLS Algorithm During SLG Fault Conditions

The decomposition diagram of zero-sequence equivalent circuit during SLG fault operation of the distribution network is shown in Fig. 4.

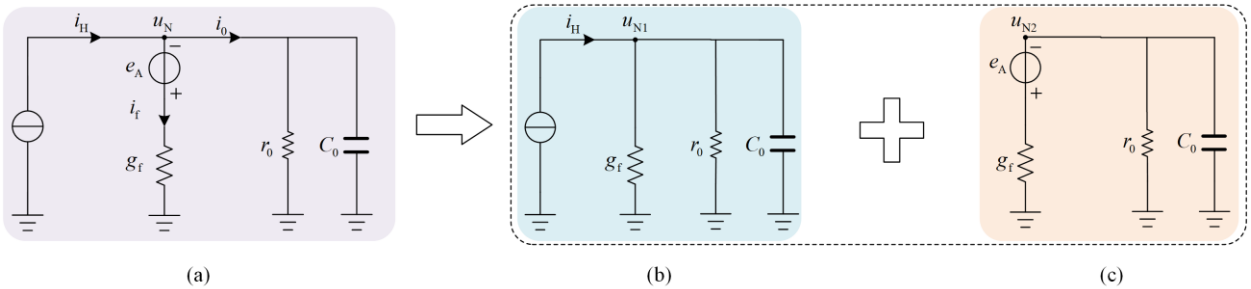

Fig. 4. Decomposition diagram of the zero-sequence equivalent circuit during SLG fault operation. (a) Zero-sequence equivalent circuit. (b) Affected only by the FASD equivalent current source. (c) Affected only by the faulty phase voltage source.

According to the superposition theorem, the zero-sequence equivalent circuit during an SLG fault can be decomposed into two parts: one influenced solely by the equivalent current source of the FASD and the other influenced solely by the faulty phase voltage source acting in conjunction with the grounding transition conductance. Similarly to (6), the Laplace expression for the injected compensating current i_H in Fig. 4(b) can be obtained as follows:

$$i_H(s) = (g_0 + sC_0 + g_f)u_{N1}(s) \tag{13}$$

The system transfer function corresponding to Fig. 4(b) can be expressed as:

$$G_1(s) = \frac{u_{N1}(s)}{i_H(s)} = \frac{1}{g_0 + g_f + sC_0} \tag{14}$$

The pulse transfer function of an open-loop system with a zero-order holder is given by:

$$G_1(z) = \frac{z^{-1}}{g_0 + g_f} \frac{1 - e^{-(g_0+g_f)T_c / C_0}}{1 - z^{-1} e^{-(g_0+g_f)T_c / C_0}} = \frac{u_{N1}(z)}{i_H(z)} \tag{15}$$

Similarly to (9), by rearranging and simplifying the coefficients of the injected compensating current and neutral point voltage in (15), there is:

$$u_{N1}(k) = a_1 i_H(k-1) - b_1 u_{N1}(k-1) \tag{16}$$

Continuing the analysis and derivation, while considering only the impact of the faulted phase source voltage as depicted in Fig. 4(c), the Laplace expression for the injected compensating current i_H in Fig. 4(c) can be obtained as follows:

$$-e_{\mathrm{A}}(s)g_{\mathrm{f}} = u_{\mathrm{N2}}(s)(g_0 + sC_0 + g_{\mathrm{f}}) \tag{17}$$

The system transfer function corresponding to Fig. 4(c) can be expressed as:

$$G_2(s) = \frac{u_{\mathrm{N2}}(s)}{e_{\mathrm{A}}(s)} = \frac{-g_{\mathrm{f}}}{g_0 + g_{\mathrm{f}} + sC_0} \tag{18}$$

The pulse transfer function of an open-loop system with a zero-order holder is given by:

$$G_2(z) = \frac{-g_{\mathrm{f}}z^{-1}}{g_0 + g_{\mathrm{f}}} \frac{1 - \mathrm{e}^{-(g_0+g_{\mathrm{f}})T_{\mathrm{c}}/C_0}}{1 - z^{-1}\mathrm{e}^{-(g_0+g_{\mathrm{f}})T_{\mathrm{c}}/C_0}} = \frac{u_{\mathrm{N2}}(z)}{e_{\mathrm{A}}(z)} \tag{19}$$

Similar to (9), by rearranging and simplifying the coefficients of the injected compensating current and neutral point voltage in (19), we can obtain that:

$$u_{\mathrm{N2}}(k) = a_2 e_{\mathrm{A}}(k-1) - b_2 u_{\mathrm{N2}}(k-1) \tag{20}$$

The system output $u_{\mathrm{N}}(k)$ can be stated as:

$$\begin{aligned} u_{\mathrm{N}}(k) = u_{\mathrm{N1}}(k) + u_{\mathrm{N2}}(k) = \\ a_1 i_{\mathrm{H}}(k-1) + a_2 e_{\mathrm{A}}(k-1) - \\ b_1 u_{\mathrm{N1}}(k-1) - b_2 u_{\mathrm{N2}}(k-1) \end{aligned} \tag{21}$$

Since u_{N1} and u_{N2} are intermediate variables that are equivalently obtained and cannot be directly measured, their estimation is substituted using the output $x_{\mathrm{a}}(k-1)$ or its estimate $\hat{x}(k-1)$ from the auxiliary model. This identification method based on substitution is referred to as the auxiliary model identification method, as shown in Fig. 5.

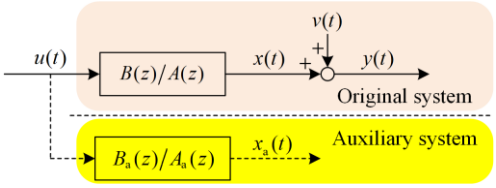

Fig. 5. Output error system with auxiliary model.

Due to T_{c} being the small sampling period approaching 0 and utilizing the equivalent infinitesimal formula, it can be inferred that:

$$\begin{cases} \lim\limits_{T_{\mathrm{c}}\to 0} a_1 = \lim\limits_{T_{\mathrm{c}}\to 0} \dfrac{1 - \mathrm{e}^{-(g_0+g_{\mathrm{f}})T_{\mathrm{c}}/C_0}}{g_0 + g_{\mathrm{f}}} = \dfrac{T_{\mathrm{c}}}{C_0} \\ \lim\limits_{T_{\mathrm{c}}\to 0} b_1 = \lim\limits_{T_{\mathrm{c}}\to 0} (-\mathrm{e}^{-(g_0+g_{\mathrm{f}})T_{\mathrm{c}}/C_0}) = -1 \\ \lim\limits_{T_{\mathrm{c}}\to 0} a_2 = \lim\limits_{T_{\mathrm{c}}\to 0} \dfrac{-g_{\mathrm{f}}}{g_0 + g_{\mathrm{f}}} (1 - \mathrm{e}^{-(g_0+g_{\mathrm{f}})T_{\mathrm{c}}/C_0}) = \dfrac{-g_{\mathrm{f}}T_{\mathrm{c}}}{C_0} \\ \lim\limits_{T_{\mathrm{c}}\to 0} b_2 = \lim\limits_{T_{\mathrm{c}}\to 0} (-\mathrm{e}^{-(g_0+g_{\mathrm{f}})T_{\mathrm{c}}/C_0}) = -1 \end{cases} \tag{22}$$

Based on the parameter identification results a_1, a_2, b_1, and b_2, the identification formulas for line-to-ground conductance, line-to-ground capacitance, and grounding transition conductance of the distribution network under SLG fault conditions can be stated as follows:

$$\begin{cases} g_0 = \dfrac{(1+b_1)(1+a_2+b_2)}{a_1(1+b_2)} \\ C_0 = T_{\mathrm{c}}/a_1 \\ g_{\mathrm{f}} = -a_2/a_1 \end{cases} \tag{23}$$

C. VFF-RLS Algorithm

The analysis in Section III.B shows that the RLS algorithm can identify the line-to-ground parameters and grounding transition conductance online during SLG fault conditions. However, the traditional RLS algorithm is disadvantaged by an unchangeable forgetting factor. In contrast, by modifying the value of the forgetting factor λ in the RLS formula, the variable forgetting factor can alter the sensitivity of the algorithm to both new and old data.

To discuss further the mechanism of the variable forgetting factor in parameter identification, define the system output $y(k)$, system input $\boldsymbol{\varphi}^{\mathrm{T}}(k)$, and system parameters $\boldsymbol{\theta}$ as follows:

$$\begin{cases} y(k) = u_{\mathrm{N}}(k) = u_{\mathrm{N1}}(k) + u_{\mathrm{N2}}(k) \\ \boldsymbol{\varphi}^{\mathrm{T}}(k) = \begin{bmatrix} i_{\mathrm{H}}(k-1) \\ e_{\mathrm{A}}(k-1) \\ -u_{\mathrm{N1}}(k-1) \\ -u_{\mathrm{N2}}(k-1) \end{bmatrix}^{\mathrm{T}} \\ \boldsymbol{\theta} = \begin{bmatrix} a_1 & a_2 & b_1 & b_2 \end{bmatrix}^{\mathrm{T}} \end{cases} \tag{24}$$

The system output, $y(k)$, can be expressed in terms of the system input $\boldsymbol{\varphi}^{\mathrm{T}}(k)$ and the system parameter $\boldsymbol{\theta}$ as follows:

$$\begin{aligned} y(k) = \boldsymbol{\varphi}^{\mathrm{T}}(k)\boldsymbol{\theta} = a_1 i_{\mathrm{H}}(k-1) + a_2 e_{\mathrm{A}}(k-1) \\ - b_1 u_{\mathrm{N1}}(k-1) - b_2 u_{\mathrm{N2}}(k-1) \end{aligned} \tag{25}$$

The formula for the RLS algorithm with a fixed forgetting factor can be written as follows:

$$\begin{cases} \hat{\boldsymbol{\theta}}(k) = \hat{\boldsymbol{\theta}}(k-1) + \boldsymbol{K}(k)\left[y(k) - \boldsymbol{\varphi}^{\mathrm{T}}(k)\hat{\boldsymbol{\theta}}(k-1) \right] \\ \boldsymbol{P}(k) = \dfrac{\left[\boldsymbol{I} - \boldsymbol{K}(k)\hat{\boldsymbol{\varphi}}^{\mathrm{T}}(k) \right]\boldsymbol{P}(k-1)}{\lambda} \\ \boldsymbol{K}(k) = \dfrac{\boldsymbol{P}(k-1)\boldsymbol{\varphi}(k)}{\lambda + \boldsymbol{\varphi}^{\mathrm{T}}(k)\boldsymbol{P}(k-1)\boldsymbol{\varphi}(k)} \\ E(k) = y(k) - \boldsymbol{\varphi}^{\mathrm{T}}(k)\hat{\boldsymbol{\theta}}(k) \end{cases} \tag{26}$$

where $\hat{\boldsymbol{\theta}}(k)$ is the estimate of the system parameters; $\boldsymbol{K}(k)$ is the gain vector; λ is the forgetting factor; $\boldsymbol{P}(k)$ is the covariance matrix; and $E(k)$ is the error between the measured value and the estimated value of the system output.

When $\lambda = 1$, it is equivalent to treating the errors at each time step in the computation equally. This implies that there is no forgetting function during the iterative calculation in the identification process. In this case, the algorithm degrades into the traditional RLS method, which has difficulty in adapting to the scenario involving disturbances to the system. When $\lambda = 0$, it means that only the error at the current time step matters in the computation, thus completely disregarding errors from past time steps. In this situation, the algorithm cannot

converge the identified parameters to stable values, resulting in ineffective estimation.

Therefore, the value of λ must be set appropriately to enhance the algorithm's performance to the highest possible extent. This paper proposes the variable forgetting factor as follows:

$$\lambda(k)=\begin{cases}\lambda_0, \text{round}\left(E^3(k)\right)=0\\ \lambda_1, \text{round}\left(E^3(k)\right)\neq 0\end{cases} \tag{27}$$

where round $(E^3(k))$ is the integer closest to $E^3(k)$. When round $(E^3(k))=0$ occurs, it signifies that the error is within an acceptable range, and $\lambda(k)=\lambda_0$. When round $(E^3(k))\neq 0$ occurs, it indicates that the error exceeds the specified threshold, and in this case, $\lambda(k)=\lambda_1$ is chosen.

By substituting $\lambda(k)$ from (27) into (26), the RLS algorithm with a fixed forgetting factor evolves into the RLS algorithm with a variable forgetting factor. The formula for the VFF-RLS can be written as:

$$\begin{cases}\hat{\boldsymbol{\theta}}(k)=\hat{\boldsymbol{\theta}}(k-1)+\boldsymbol{K}(k)\left[y(k)-\boldsymbol{\varphi}^{\mathrm{T}}(k)\hat{\boldsymbol{\theta}}(k-1)\right]\\ \boldsymbol{P}(k)=\dfrac{\left[\boldsymbol{I}-\boldsymbol{K}(k)\hat{\boldsymbol{\varphi}}^{\mathrm{T}}(k)\right]\boldsymbol{P}(k-1)}{\lambda(k)}\\ \boldsymbol{K}(k)=\dfrac{\boldsymbol{P}(k-1)\boldsymbol{\varphi}(k)}{\lambda(k)+\boldsymbol{\varphi}^{\mathrm{T}}(k)\boldsymbol{P}(k-1)\boldsymbol{\varphi}(k)}\\ E(k)=y(k)-\boldsymbol{\varphi}^{\mathrm{T}}(k)\hat{\boldsymbol{\theta}}(k)\\ \lambda(k)=\begin{cases}\lambda_0, \text{round}(E^3(k))=0\\ \lambda_1, \text{round}(E^3(k))\neq 0\end{cases}\end{cases} \tag{28}$$

The online identification scheme based on the VFF-RLS algorithm is shown in Fig. 6.

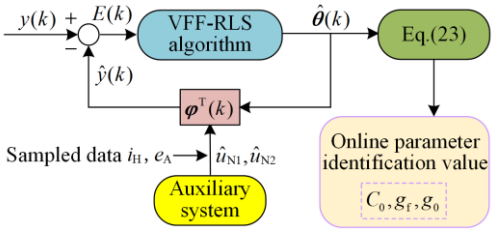

Fig. 6. Online identification scheme based on the VFF-RLS algorithm.

As Fig. 6 shows, combining the sampled data i_{H}, e_{A} and the auxiliary system output $\hat{u}_{\mathrm{N1}}, \hat{u}_{\mathrm{N2}}$ into the system input matrix $\boldsymbol{\varphi}^{\mathrm{T}}(k)$ and performing matrix multiplication between $\boldsymbol{\varphi}^{\mathrm{T}}(k)$ and the estimated value of the system parameters $\hat{\boldsymbol{\theta}}(k)$ yields the estimated value of the system output $\hat{y}(k)$. Calculating $y(k)-\hat{y}(k)$ results in $E(k)$, and adjusting the forgetting factor of the VFF-RLS algorithm based on the magnitude of $E(k)$, obtain the corresponding estimated value of the system parameters $\hat{\boldsymbol{\theta}}(k)$. Finally, the online parameter identification value C_0, g_{f}, g_0 are derived according to (23).

IV. Simulation and Discussion

A. Simulation Model

To validate the proposed online identification method based on the VFF-RLS algorithm, a simulation model of a 10 kV distribution network with an FASD is constructed in MATLAB/Simulink. Figure 7 depicts the schematic diagram of the 10 kV distribution network simulation model. Three feeder lines are drawn from the bus, and phase A of feeder line FL1 experiences an SLG fault. The simulation parameters are listed in Table I.

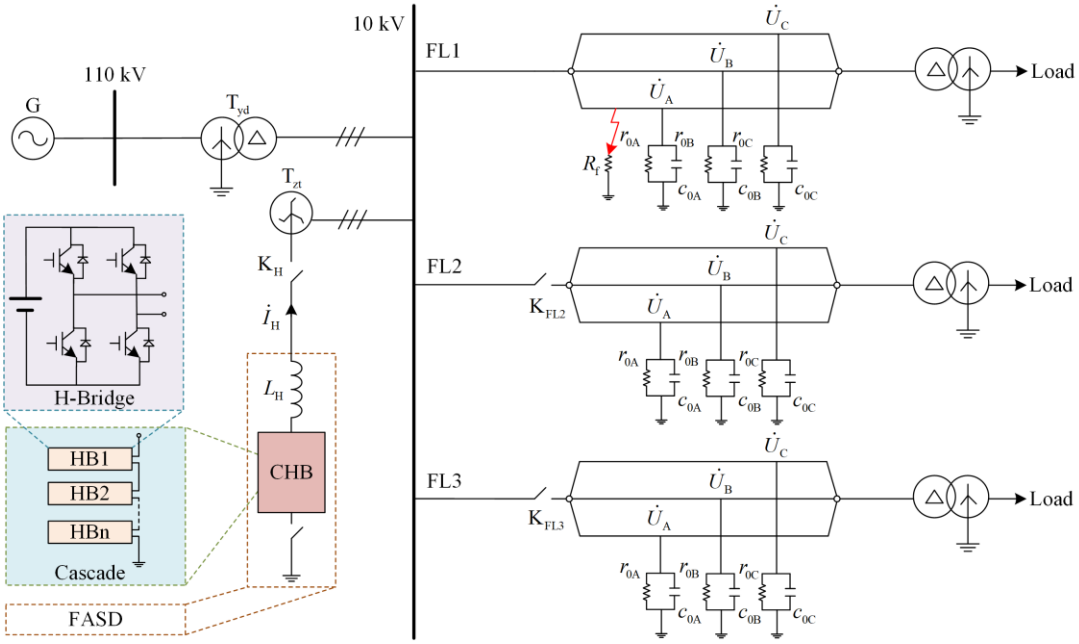

Fig. 7. Simulation model of 10 kV distribution network with the FASD.

TABLE I
SIMULATION PARAMETERS

Description	Value
Voltage source G of distribution network (kV)	110
Cascaded numbers	10
Filter inductance (H)	0.01
Sampling frequency (kHz)	100
DC-link voltage of each HB (V)	900
Line-to-ground resistance r_0 (kΩ)	10
Line-to-ground capacitance C_0 of FL1 (μF)	21
Line-to-ground capacitance C_0 of FL2 (μF)	20
Line-to-ground capacitance C_0 of FL3 (μF)	10

B. Arc Suppression Effect Based on the VFF-RLS Algorithm

Considering that the identification accuracy of the line-to-ground resistance in line-to-ground parameters only has a limited impact on the accuracy of compensation current calculation, this secondary factor is neglected and only the online identification of the line-to-ground capacitance is considered.

For the 10 kV distribution network, a SLG fault occurs at $t_1 = 0.01$ s, and the FASD is activated at $t_2 = 0.07$ s. Figure 8 and Table II provide the identification results of the line-to-ground capacitance under four different grounding transition resistance scenarios, along with their corresponding arc suppression effects. Assuming that the residual current at the SLG fault point after the fault is $I_{\mathrm{f}}^{\mathrm{amp}}$, and the residual current at the fault point after compensation by the arc suppression device is $I_{\mathrm{res}}^{\mathrm{amp}}$, the SLG fault point residual current suppression rate φ is defined as follows:

$$\varphi = \frac{I_{\mathrm{f}}^{\mathrm{amp}} - I_{\mathrm{res}}^{\mathrm{amp}}}{I_{\mathrm{f}}^{\mathrm{amp}}} \times 100\% \tag{29}$$

As seen from Fig. 8 and Table II, the FASD can dynamically adjust the magnitude of injected compensating current in various grounding transition resistance scenarios, leading to significant reductions in the SLG fault point currents after injecting currents. Under different grounding transition resistance values, the relative error of the distribution line-to-ground capacitance remains within 0.1% and the SLG fault point residual current suppression rate φ reaches more than 99%.

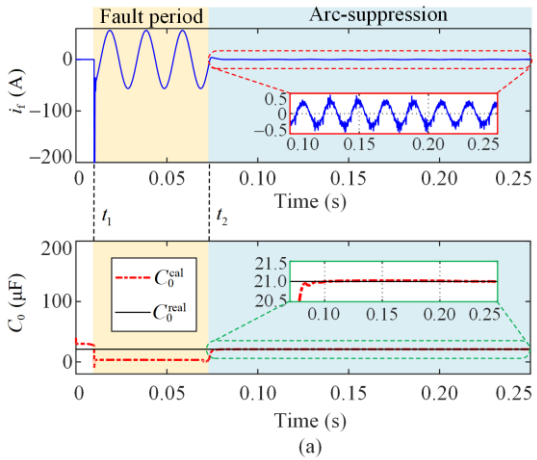

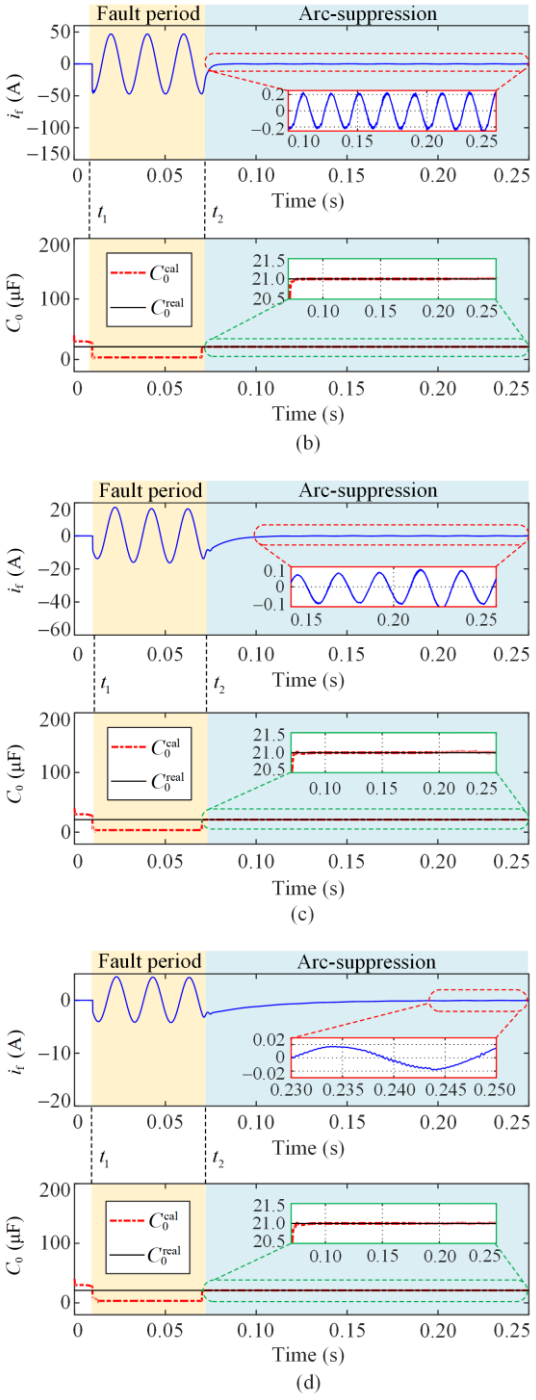

Fig. 8. Arc suppression effect and identification of line-to-ground capacitance under different grounding transition resistances. (a) R_{f} =10 Ω. (b) R_{f} =100 Ω. (c) R_{f} =500 Ω. (d) R_{f} =2000 Ω.

In summary, the VFF-RLS algorithm can swiftly and accurately perceive line-to-ground capacitance values under different grounding transition resistance values. The identification values are fed back into (4) to achieve timely SLG fault point current compensation.

TABLE II
SPECIFIC LINE-TO-GROUND CAPACITANCE IDENTIFICATION VALUE AND ARC SUPPRESSION EFFECT

R_f (Ω)	C_0^{cal} (μF)	Error (%)	I_f^{amp} (A)	I_{res}^{amp} (A)	φ (%)
10	21.001	0.005	56.486	0.458	99.189
100	21.018	0.086	46.935	0.232	99.506
500	21.010	0.048	17.306	0.112	99.353
2000	21.010	0.048	4.458	0.020	99.551

C. Fault Type Discrimination based on the VFF-RLS Algorithm

According to the analysis of Section IV.B, the VFF-RLS algorithm can identify the line-to-ground capacitance value online and correct the injected current value in real time to achieve good arc suppression effects.

To verify that the fault type can be distinguished according to the grounding transition conductance identification value, a scenario is introduced where the SLG fault disappears at 0.12 s. Figure 9 shows the change in grounding transition conductance after an SLG fault. This demonstrates that, after injecting the current, the online identification value of grounding transition conductance can reach stability within 0.01 s, indicating that the VFF-RLS algorithm can track changes in the grounding transition conductance in real time. When the SLG fault disappears, the online identification value of grounding transition conductance drops to nearly 0 within 0.01 s for conductances of 10 Ω and 100 Ω, and within 0.04 s for 2000 Ω. Therefore, by setting a threshold, the disappearance of the SLG fault can be quickly detected, enabling accurate identification of the fault type.

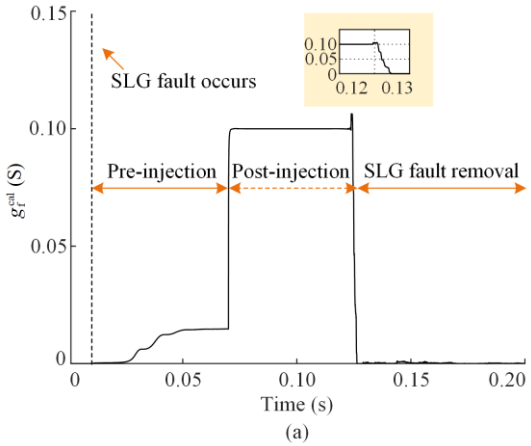

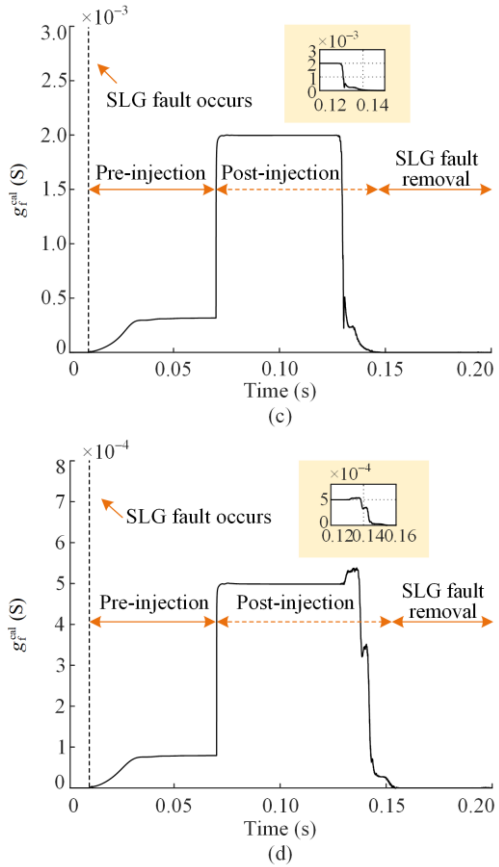

Fig. 9. Grounding transition conductance identification based on the VFF-RLS algorithm. (a) $R_f = 10\,\Omega$. (b) $R_f = 100\,\Omega$. (c) $R_f = 500\,\Omega$. (d) $R_f = 2000\,\Omega$.

Table III provides the specific grounding transition conductance identification value and T_d. T_d is defined as the time it takes for the grounding transition conductance value to drop below the threshold after the disappearance of the SLG fault.

From Table III, the identification errors for the four different grounding transition conductance values are all $<$ 1%, which is well within acceptable limits for fault type discrimination. Additionally, the time interval from the occurrence of the SLG fault to the moment when the grounding transition conductance identification value drops below the threshold is within 0.04 s. This indicates the feasibility of fault type discrimination based on the comparison between the grounding transition conductance value and the threshold. Notably, setting the threshold ε is exceptionally convenient, and even for a 2000 Ω SLG fault, the grounding transition conductance value can reach 0.0005 S, and the threshold's order of magnitude can be set lower, e.g., with 100 kΩ as the boundary, while the threshold can be configured with a value less than a magnitude of −5.

TABLE III
SPECIFIC GROUNDING TRANSITION CONDUCTANCE IDENTIFICATION VALUE AND T_d

$R_f(\Omega)$	$g_f^{cal}(S)$	$R_f^{cal}(\Omega)$	Error (%)	$T_d(s)$
10	9.990×10^{-2}	10.010	0.100	0.005
100	9.969×10^{-3}	100.311	0.310	0.010
500	1.988×10^{-3}	503.018	0.604	0.022
2000	4.986×10^{-4}	2005.616	0.281	0.035

In summary, the flow chart of the FASD deactivation scheme is shown in Fig. 10.

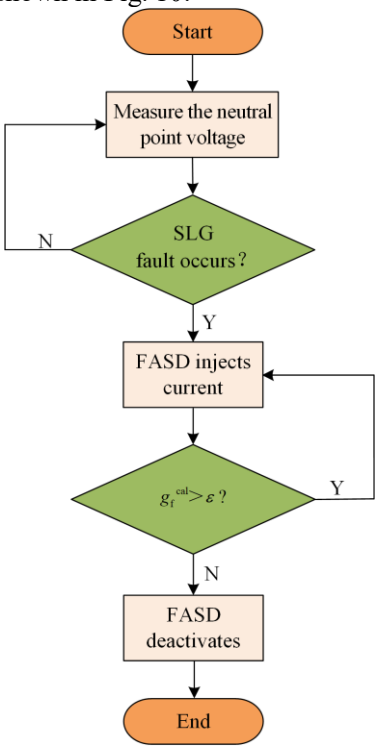

Fig. 10. Flow chart of the FASD deactivation scheme.

When an SLG fault occurs, the FASD begins injecting current and calculates the grounding transition conductance value. If the grounding transition conductance value is greater than the threshold, it indicates that the SLG fault has not disappeared, and the FASD continues to inject current. If the grounding transition conductance value falls below the threshold, it indicates that the SLG fault has been cleared, and the fault is immediately classified as transient. The FASD can then be deactivated and the overvoltage risk in the non-faulted phase devices can be significantly reduced.

D. Comparative Analysis of the VFF-RLS Algorithm with other Algorithms

This section analyzes the VFF-RLS algorithm's performance by comparing with other algorithms. Assuming the SLG fault occurs at $t_1 = 0.01$ s, the arc suppression device is activated at $t_2 = 0.07$ s, and line switching occurs at $t_3 = 0.18$ s.

Figure 11 and Table IV compare the residual current suppression rates and the convergence of the online identification values of line-to-ground capacitance when using the RLS algorithm and VFF-RLS algorithm in line-switching scenarios. The interval $t_2 - t_3$ in Fig. 11 is defined as the first arc suppression segment, where line switching occurs at t_3. The interval $t_3 - t_4$ represents the identification convergence region and the total convergence time for the identification convergence region is defined as $t_{con} = t_4 - t_3$. Assuming the residual current at the moment of line switching is I_{res1}^{amp}, and after secondary compensation by the arc suppression device is I_{res2}^{amp}, the second residual current suppression rate φ_2 is defined as:

$$\varphi_2 = \frac{I_{res1}^{amp} - I_{res2}^{amp}}{I_{res1}^{amp}} \times 100\% \tag{30}$$

As shown in Fig. 11, the two algorithms exhibit different response performances during the line-switching disturbance scenario. The RLS algorithm requires a longer time to achieve convergence in line-to-ground capacitance identification. This implies that the RLS algorithm also needs more time for the second residual current suppression in response to the sudden increase in residual current. Conversely, due to the variable forgetting factor strategy, the VFF-RLS algorithm converges more rapidly in line-to-ground capacitance identification compared to the RLS algorithm. Consequently, it quickly executes the second suppression of the SLG fault current, preventing the SLG fault from further escalation.

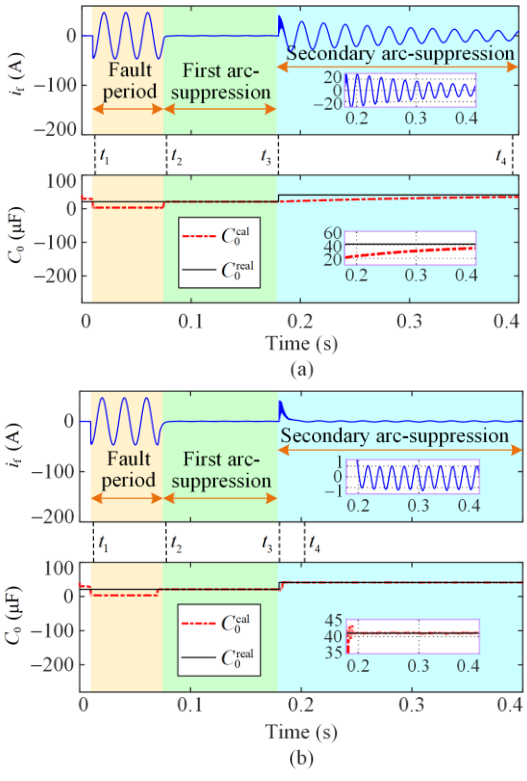

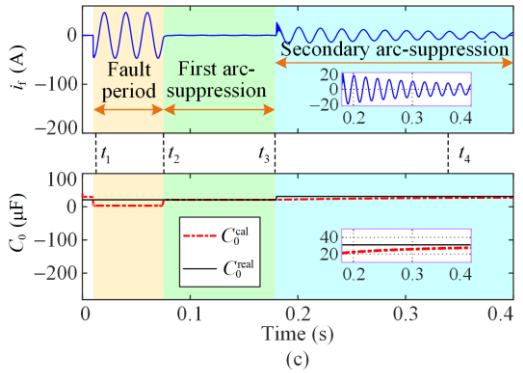

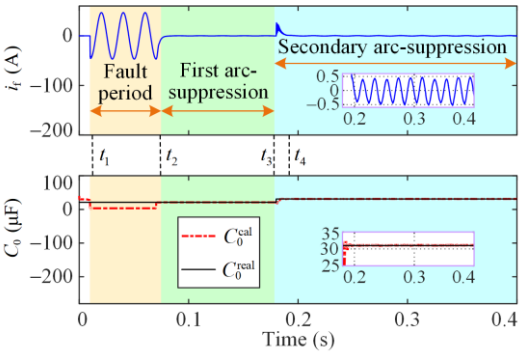

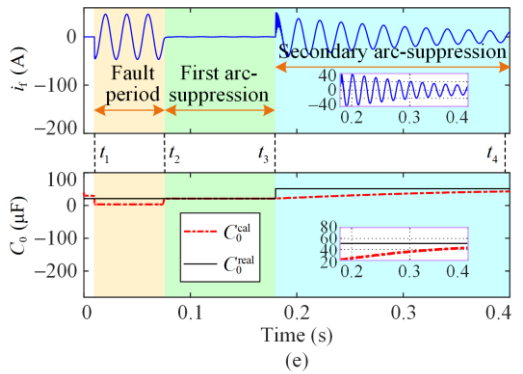

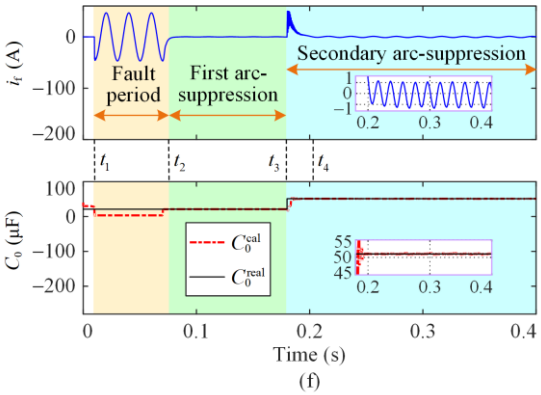

Fig. 11. Comparison of arc suppression effect and identification of line-to-ground capacitance between the RLS algorithm and the VFF-RLS algorithm during line switching in the arc suppression period. (a) FL2 switching (RLS). (b) FL2 switching (VFF-RLS). (c) FL3 switching (RLS). (d) FL3 switching (VFF-RLS). (e) FL2+FL3 switching (RLS). (f) FL2+FL3 switching (VFF-RLS).

Table IV provides a detailed comparison of the convergence time and second residual current suppression rate between the RLS and VFF-RLS algorithms. From the convergence-time perspective, when line FL2 undergoes switching, the RLS algorithm takes 0.21 s to converge, while the VFF-RLS algorithm only takes 0.02 s. For line FL3 switching, the convergence time of the RLS algorithm is 0.16 s, whereas it remains at 0.01 s for the VFF-RLS algorithm. When both line FL2 and line FL3 undergo switching simultaneously, the RLS algorithm's convergence time is 0.21 s, compared to 0.02 s for the VFF-RLS algorithm. This indicates that the VFF-RLS algorithm converges faster in the line-switching scenario. Comparing the RLS and VFF-RLS algorithms, the latter can more quickly suppress the second residual current caused by line switching. The second residual current suppression rate of the VFF-RLS algorithm consistently exceeds 97%, while the RLS algorithm only reaches approximately 75%.

TABLE IV
THE CONVERGENCE TIME AND SECOND RESIDUAL CURRENT SUPPRESSION RATE OF RLS AND VFF-RLS ALGORITHMS

Method	Switching line	t_{con} (s)	I_{res1}^{amp} (A)	I_{res2}^{amp} (A)	φ_2 (%)
RLS	FL2	0.21	26.296	6.679	74.601
	FL3	0.16	40.952	10.266	74.932
	FL2+FL3	0.21	50.035	12.013	75.991
VFF-RLS	FL2	0.02	26.313	0.524	98.009
	FL3	0.01	41.022	1.101	97.316
	FL2+FL3	0.02	50.096	1.348	97.309

To summarize, under changing line operating conditions, the VFF-RLS algorithm demonstrates better adaptability compared to the RLS algorithm. However, the flexibility of the algorithm usually comes at the cost of robustness, i.e., the more flexible the algorithm, the lower the robustness. Therefore, further analysis on the robustness of the VFF-RLS algorithm is conducted.

Assuming the system input, $\boldsymbol{\varphi}^{\mathrm{T}}(k)$, is disturbed by Gaussian noise with different means μ and variances σ, an SLG fault occurs in the distribution network at 0.01 s and the FASD starts injecting current at 0.07 s. The identification of line-to-ground capacitance based on the VFF-RLS algorithm is shown in Fig. 12 and Table V.

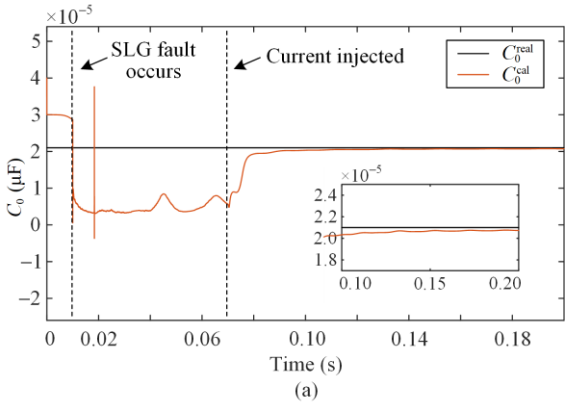

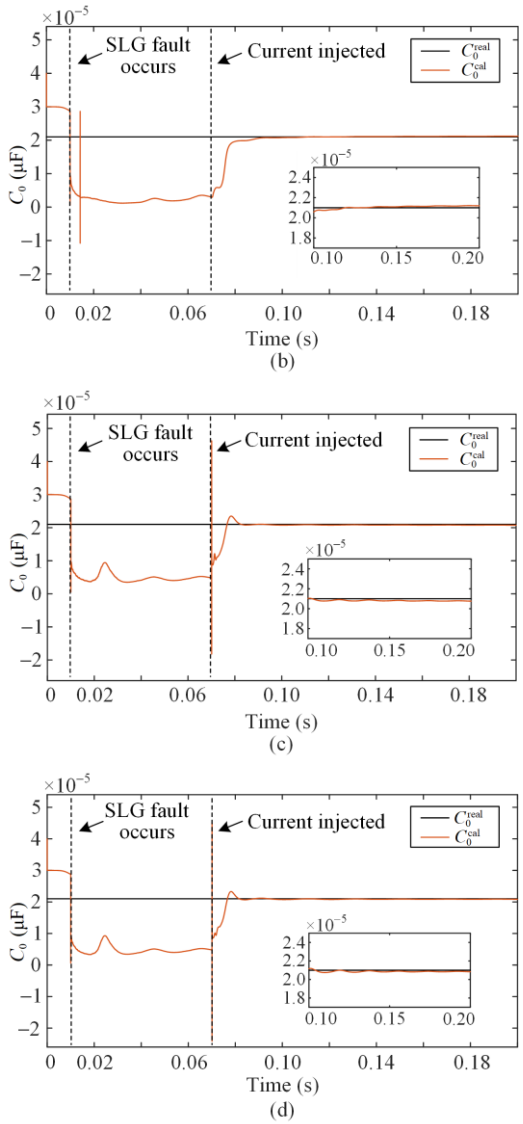

Fig. 12. Online identification of line-to-ground capacitance of VFF-RLS algorithm under Gaussian noise interference. (a) $\mu = 0.15, \sigma = 0.1$. (b) $\mu = 0.25, \sigma = 0.1$. (c) $\mu = 0.25, \sigma = 0.2$. (d) $\mu = 0.4, \sigma = 0.25$.

TABLE V
ACCURACY OF LINE-TO-GROUND CAPACITANCE IDENTIFICATION UNDER NO NOISE INTERFERENCE AND GAUSSIAN NOISE INTERFERENCE

Noise type	Noise parameters	Accuracy (%)
No noise interference	None	99.91
Gaussian noise interference	$\mu = 0.15, \sigma = 0.1$	98.71
	$\mu = 0.25, \sigma = 0.1$	99.10
	$\mu = 0.25, \sigma = 0.2$	98.86
	$\mu = 0.4, \sigma = 0.25$	99.24

Figure 12 and Table V show that the accuracy of line-to-ground capacitance identification remains largely unaffected by the interference of Gaussian noise with different means and variances. The identified values can still quickly approximate the true values, and the identification accuracy remains above 98%. This demonstrates the robustness of the VFF-RLS algorithm.

To further illustrate the advantages of the VFF-RLS algorithm, the online identification accuracy and arc suppression effect of the VFF-RLS algorithm are compared with [1], [10], and [22]. In [1], a flexible arc suppression method for distribution networks with a neutral point grounded via FASD is introduced. The effectiveness of the proposed method is demonstrated by comparing the residual current of the SLG fault before and after arc suppression. In [10], a new method for measuring line-to-ground parameters in distribution networks is presented, achieving accurate measurements through secondary current injection. Reference [22] proposes a method for identifying grounding faults in distribution networks based on transition conductance, which executes fault detection by online tracking of the transition conductance value. The specific comparison results are presented in Table VI in which 'Y' represents 'yes', and 'N' represents 'no'.

TABLE VI
COMPARISON OF THE VFF-RLS ALGORITHM WITH OTHER ALGORITHMS

Method	R_f (Ω)	Algorithm performance			Additional measuring device?	Adapt to changes in line structure?	Online identification?
		Identification error of C_0(%)	Identification error of g_f(%)	φ (%)			
VFF-RLS	10	0.005	0.100	99.189	N	Y	Y
	100	0.086	0.310	99.506			
	500	0.048	0.604	99.353			
	2000	0.048	0.281	99.551			
Method in [1]	10	N	N	98.077	Y	N	N
	100			99.388			
	500			98.953			
	1000			98.767			
Method in [10]	N	0.45	N	N	Y	N	N
Method in [22]	500	0.3119	5.55	N	Y	N	N
	2000		1.28				
	4000		8.90				

As Table VI shows, compared to the method proposed in [1], the VFF-RLS algorithm achieves a higher residual current suppression rate and can better adapt to changes in line structure. In comparison to the method from [10], the VFF-RLS algorithm achieves online identification of line-to-ground parameters without additional measuring devices with higher identification accuracy. When compared to the method proposed in [22], the VFF-RLS algorithm enables online identification of grounding transition conductance without additional measuring devices, providing higher identification accuracy and thus enabling more reliable fault type discrimination.

In summary, the VFF-RLS algorithm integrates online identification of line-to-ground parameters, SLG fault arc suppression, and fault type discrimination into FASD. It addresses previous limitations, including the need for additional measurement devices, poor adaptivity to changes in line structure, and the inability to perform online identification.

V. Conclusion

This paper presents online identification methods of distribution line-to-ground parameters and grounding transition conductance during arc suppression. The following conclusions can be drawn from the studies:

1) By utilizing the neutral point voltage of the distribution network and the injected current from FASD, the line-to-ground parameters and the grounding transition conductance of the distribution network can be identified online without the need for additional measuring devices. This reduces both cost and the impact of injecting a specific frequency current into the distribution network.

2) The VFF-RLS algorithm can adapt to changes in line structure and dynamically adjust the current injected by FASD in real time. The adjustment is based on the online identification of the line-to-ground parameters to ensure effective arc suppression. The fault type is determined online using the identified grounding transition-conductance. As a result, the FASD can be promptly disengaged, reducing the risk of overvoltage in non-faulted phase devices.

Acknowledgment

Not applicable.

Authors' Contributions

Zeyin Zheng: supervision, conceptualization, writing-review & editing. Jianfeng Xu: formal analysis, writing original draft, methodology, and validation. Moufa Guo: project administration, resources, and funding acquisition. All authors read and approved the final manuscript.

Funding

This work is supported in part by the National Natural Science Foundation of China (No. 51677030) and in part by the Natural Science Foundation of Fujian Province, China (No. 2023J05106).

Availability of Data and Materials

Not applicable.

Declarations

Competing interests: The authors declare that they have no known competing financial interests or personal relationships that could have appeared to influence the work reported in this article.

Authors' Information

Zeyin Zheng received the B.S. degree in electrical engineering from Fuzhou University, Fuzhou, China, in 2014, and the Ph.D. degree in electrical engineering from Yuan Ze University, Taoyuan, Taiwan, China in 2021. He has been with Fuzhou University, where he is currently an associate professor with the college of Electrical Engineering and Automation. His research interests include power distribution systems and automation.

Jianfeng Xu received the B.S. degree in electrical engineering from Fuzhou University, Fuzhou, China, in 2018. He has been with Fuzhou University, where he is currently a master student with the college of Electrical Engineering and Automation. His research interests include power distribution systems and automation.

Moufa Guo received the B.S. and M.S. degrees in electrical engineering from Fuzhou University, Fuzhou, China, in 1996 and 1999, respectively, and the Ph.D. degree in electrical engineering from Yuan Ze University, Taoyuan, Taiwan, China in 2018. Since 2000, he has been with Fuzhou University, where he is currently a professor with the College of Electrical Engineering and Automation. His research interests include the information processing, protection control and flexible arc suppression of single-line-to-ground fault in distribution networks.

References

[1] Z. Zheng, M. Guo, and N. Yang *et al*., "Single-phase flexible arc suppression device based on BSC-SOGI-PLL method for distribution networks," *International Journal of Electrical Power and Energy Systems*, vol. 121, Oct. 2020.

[2] Y. Xiao, J. Ouyang, and X. Xiong *et al*., "Fault protection method of single-phase break for distribution network considering the influence of neutral grounding modes," *Protection and Control of Modern Power Sys-*

tems, vol. 5, no. 2, pp. 1-13, Apr. 2020.

[3] C. Jia, L. Yang, and G. Du, "Review of key technologies on full current compensation arc suppression coil," *Power System Protection and Control*, vol. 43, no. 9, pp. 145-154, May 2015. (in Chinese)

[4] S. Ai, X. Li, and W. Li *et al*., "Arc suppression technology based on fast switch for distribution network," *High Voltage Apparatus*, vol. 53, no. 3, pp. 178-184, Mar. 2017. (in Chinese)

[5] F. Zhang, Y. Xue, and B. Xu, "A method for calculating residual current in a resonant grounding system based on signal injection," *Power System Protection and Control*, vol. 51, no. 13, pp. 132-138, Jul. 2023. (in Chinese)

[6] P. Wang, B. Chen, and C. Tian *et al*., "A novel neutral electromagnetic hybrid flexible grounding method in distribution networks," *IEEE Transactions on Power Delivery*, vol. 32, no. 3, pp. 1350-1358, Jun. 2017.

[7] X. Wang, N. Li, and X. Su *et al*., "Analysis on earth fault protection malfunction of generator with arc suppression coil grounding," *Power System Protection and Control*, vol. 44, no. 7, pp. 140-144, Apr. 2016. (in Chinese)

[8] B. Wu, G. Chen, and Y. Jin *et al*., "A new type of arc-suppression coil automatic tracking compensation device," *Power System Protection and Control*, vol. 46, no. 19, pp. 151-157, Oct. 2018. (in Chinese)

[9] L. He, L. Ge, and B. Sun, "Measurement of line-to-ground capacitance in distribution network considering magnetizing impedance's frequency characteristic," *Energies*, vol. 10, no. 4, Apr. 2017.

[10] Z. Zheng, M. Guo, and T. Jin *et al*., "A novel method of insulation parameters measurement based on hybrid flexible arc suppression device in distribution networks," *International Journal of Electrical Power and Energy Systems*, vol. 130, Sep. 2021.

[11] G. Zhao, K. Chen, and W. Zeng *et al*., "Performance analysis and design of an arc suppression inverter considering equivalent load change," *Power System Protection and Control*, vol. 51, no. 1, pp. 148-157, Jan. 2023. (in Chinese)

[12] H. Wu, Y. Yuan, and K. Ma *et al*., "Estimate the probability distribution of imbalance-induced energy loss with minimal data," *IEEE Transactions on Power Systems*, vol. 36, no. 4, pp. 3798-3801, Jul. 2021.

[13] S. Dahal and H. Salehfar, "Impact of distributed generators in the power loss and voltage profile of three phase unbalanced distribution network," *International Journal of Electrical Power and Energy Systems*, vol. 77, pp. 256-262, May 2016.

[14] Z. He, Z. Yang, and X. Cui, *et al*., "A method of state-of-charge estimation for EV power lithium-ion battery using a novel adaptive extended Kalman filter," *IEEE Transactions on Vehicular Technology*, vol. 69, no. 12, pp. 14618-14630, Dec. 2020.

[15] H. Liu, F. Hu, and J. Su *et al*., "Comparisons on Kalman-filter-based dynamic state estimation algorithms of power systems," *IEEE Access*, vol. 8, pp. 51035-51043, Mar. 2020.

[16] W. Ge, Y. Cai, and J. Li *et al*., "Three-phase state estimation of a distribution network based on multi-branch current mixing measurement," *Power System Protection and Control*, vol. 48, no. 9, pp. 1-10, May 2020. (in Chinese)

[17] S. Xu, H. Liu, and T. Bi *et al*., "An improved Taylor weighted least squares method for estimating synchrophasor," *International Journal of Electrical Power and Energy Systems*, vol. 120, Sep. 2020.

[18] J. Khodaparast and M. Khederzadeh, "Least square and Kalman based methods for dynamic phasor estimation: a review," *Protection and Control of Modern Power Systems*, vol. 2, no. 1, pp. 1-18, Jan. 2017.

[19] K. Anjaiah, P. K. Dash, and M. Sahani, "A new protection scheme for PV-wind based DC-ring microgrid by using modified multifractal detrended fluctuation analysis," *Protection and Control of Modern Power Systems*, vol. 7, no. 1, pp. 100-123, Jan. 2022.

[20] Q. Song, Y. Mi, and W. Lai, "A novel variable forgetting factor recursive least square algorithm to improve the anti-interference ability of battery model parameters identification," *IEEE Access*, vol. 7, pp. 61548-61557, Jan. 2019.

[21] Z. Zheng, M. Guo, and N. Yang *et al*., "Flexible arc-suppression method based on improved distributed commutations modulation for distribution networks," *International Journal of Electrical Power and Energy Systems*, vol. 116, Mar. 2020.

[22] Z. Wu, M. Fang, and J. Cai *et al*., "Single-phase grounding fault identification based on transition conductance tracking method," *Mathematical Problems in Engineering*, vol. 2022, Oct. 2022.